Cancer and Metastasis Reviews (2019) 38:51–64
https://doi.org/10.1007/s10555-019-09788-3

Molecular and functional imaging insights into the role of hypoxia in cancer aggression

Samata Kakkad[1] · Balaji Krishnamachary[1] · Desmond Jacob[1] · Jesus Pacheco-Torres[1] · Eibhlin Goggins[1] · Santosh Kumar Bharti[1] · Marie-France Penet[1,2] · Zaver M. Bhujwalla[1,2,3]

Published online: 6 March 2019
© Springer Science+Business Media, LLC, part of Springer Nature 2019

Abstract
Hypoxia in cancers has evoked significant interest since 1955 when Thomlinson and Gray postulated the presence of hypoxia in human lung cancers, based on the observation of necrosis occurring at the diffusion limit of oxygen from the nearest blood vessel, and identified the implication of these observations for radiation therapy. Coupled with discoveries in 1953 by Gray and others that anoxic cells were resistant to radiation damage, these observations have led to an entire field of research focused on exploiting oxygenation and hypoxia to improve the outcome of radiation therapy. Almost 65 years later, tumor heterogeneity of nearly every parameter measured including tumor oxygenation, and the dynamic landscape of cancers and their microenvironments are clearly evident, providing a strong rationale for cancer personalized medicine. Since hypoxia is a major cause of extracellular acidosis in tumors, here, we have focused on the applications of imaging to understand the effects of hypoxia in tumors and to target hypoxia in theranostic strategies. Molecular and functional imaging have critically important roles to play in personalized medicine through the detection of hypoxia, both spatially and temporally, and by providing new understanding of the role of hypoxia in cancer aggressiveness. With the discovery of the hypoxia-inducible factor (HIF), the intervening years have also seen significant progress in understanding the transcriptional regulation of hypoxia-induced genes. These advances have provided the ability to silence HIF and understand the associated molecular and functional consequences to expand our understanding of hypoxia and its role in cancer aggressiveness. Most recently, the development of hypoxia-based theranostic strategies that combine detection and therapy are further establishing imaging-based treatment strategies for precision medicine of cancer.

Keywords Hypoxia · Imaging · Vascularization · Metastasis · Theranostics

1 Introduction

Oxygen is critically important for cellular metabolism and energy production in mammalian cells. Imbalances in oxygen tensions are encountered during mammalian development and embryogenesis [1], in heart disease [2], in chronic obstructive pulmonary disorders [3], in wound healing [4], and in cancers [5]. In cancers, the uncontrolled proliferation of cancer cells in combination with the chaotic neovasculature results in the development of chronic diffusion-limited hypoxia [6]. Immature blood vessels and increased tumor interstitial pressure can also result in vascular collapse causing acute or intermittent hypoxia [6]. Intermittent hypoxia has been identified as a potential driver of somatic evolution and a cause of tumor genetic and physiologic heterogeneity [7]. Hypoxia results in the upregulation of vascular endothelial growth factor (VEGF) [8] leading to increased angiogenesis, neovascularization, and reoxygenation of hypoxic regions. Reoxygenation also occurs due to therapy-induced cell death because increased nutrients and oxygen become available to the remaining cells [9–12].

Oxygen homeostasis in mammalian cells is maintained through transcriptional activation by the hypoxia-inducible

Samata Kakkad and Balaji Krishnamachary contributed equally to this work.

✉ Zaver M. Bhujwalla
zaver@mri.jhu.edu

[1] Division of Cancer Imaging Research, The Russell H. Morgan Department of Radiology and Radiological Science, The Johns Hopkins University School of Medicine, 720 Rutland Avenue, Rm 208C Traylor Building, Baltimore, MD 21205, USA

[2] Sidney Kimmel Comprehensive Cancer Center, The Johns Hopkins University School of Medicine, Baltimore, MD, USA

[3] Department of Radiation Oncology and Molecular Radiation Sciences, The Johns Hopkins University School of Medicine, Baltimore, MD, USA

factor (HIF) [13], a heterodimer that is composed of two subunits HIF-1α and HIF-1β [14], as shown in the schematic in Fig. 1. HIF-1α is ubiquitinated under well-oxygenated conditions by the von Hippel-Lindau (VHL) protein. The VHL protein binds to hydroxylated proline residues, recruiting ubiquitin ligase to degrade HIF-1α in the oxygen-dependent degradation domain of HIF-1α [15]. Under hypoxic conditions, HIF-1α is stabilized due to the inhibition of prolyl hydroxylases [16]. Stabilized HIF-1α binds to HIF-1β and is translocated into the nucleus. In the nucleus, HIF functions as a transcription factor by recognizing and binding to the hypoxia response element (HRE) that consists of the core sequence 5′-RCGTG-3′ on the promoter region of target genes such as carbonic anhydrase IX (CAIX) [14, 17]. Two additional isoforms, HIF-2α and HIF-3α, have also been identified [15, 18]. HIF-1α transcriptional activation is triggered by short-term hypoxia of 2–24 h with oxygen tensions < 0.1% O_2, while HIF-2α transcriptional activation occurs under milder hypoxic conditions (< 5% O_2) and is active over a period of 48–72 h [19, 20]. As shown in the schematic in Fig. 1, HIF transcriptionally activates select genes that assist cancer cells to adapt to hypoxia by increasing angiogenesis, modifying metabolism, and increasing survival and proliferation [21, 22]. An increase of HIF can also occur due to oncogenic mutations in phosphatase and tensin homolog (PTEN), succinate dehydrogenase [23], fumarate hydratase, genetic mutation or loss of both alleles of the VHL gene [24, 25], activation of phosphoinositide 3 kinase (PI3K)/Akt/mammalian target of the rapamycin apoptosis pathway [26], or due to epigenetic changes [27, 28]. Several preclinical and human studies have identified the role of hypoxia in tumor aggressiveness, resistance to chemo and radiation therapy, remodeling of the extracellular matrix (ECM), invasion, and metastasis [29–33]. Radiosensitivity starts to decrease at oxygen tensions below 15 mmHg or 2% O_2 [34].

Hypoxia is a major cause of the acidic extracellular pH (pHe) of tumors due to increased glycolysis that, coupled with the poor perfusion in hypoxic tumor areas, leads to an accumulation of H^+ ions ([35] and the references therein). However, acidic pHe can occur independently of hypoxia due to increased expression of H^+-ATPases and Na^+/H^+ exchangers ([36] and the references therein). Extracellular acidosis results in increased cancer invasion in pathways both dependent and independent of hypoxia [35]. HIF-2α has been

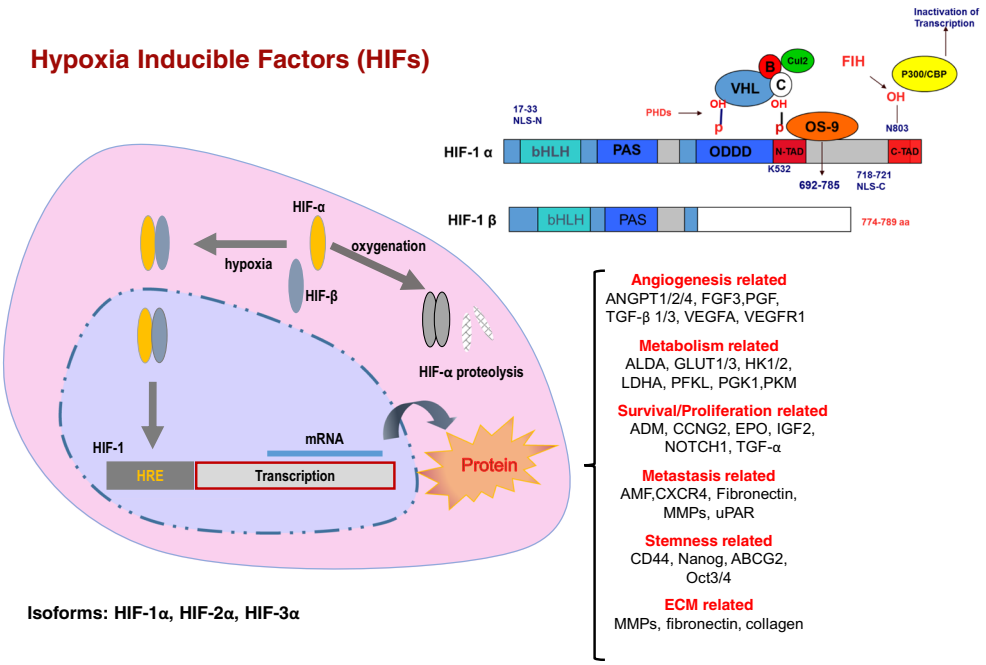

Fig. 1 Schematic figure summarizing the HIF pathway and the transcriptional regulation by HIF of genes related to angiogenesis, metabolism, survival/proliferation, metastasis, stemness, and the ECM. Top right: Box and line diagram representing the domain structure of HIF-1α (above) and HIF-1β (below) proteins. Oxygen sensing is achieved by hydroxylation of proline residues present in the oxygen-dependent degradation (ODD) domain of the HIF-1α protein. Further recruitment of VHL and ubiquitin proteins to the hydroxylated protein results in the proteosomal degradation of HIF-1α under normoxia. The schematic on the left shows the transcriptional activity of HIF in response to hypoxia resulting in the activation of proteins that actively play a role in tumor progression. ANGPT1/2/4, angiopoietin-1/2/4; FGF3, fibroblast growth factor receptor 3; PGF, placental growth factor; TGF-β 1/3, transforming growth factor beta 1/3; VEGFA, vascular endothelial growth factor A; VEGFR1, vascular endothelial growth factor receptor 1; ALDA, aldolase A; GLUT1/3, glucose transporter 1/3; HK1/2, hexokinase1/2; LDHA, lactate dehydrogenase A; PFKL, 6-phosphofructokinase, liver type; PGK1, phosphoglycerate kinase 1; PKM, pyruvate kinase muscle isozyme; ADM, adrenomedullin; CCNG2, cyclin G2; EPO, erythropoietin; IGF2, insulin-like growth factor 2; NOTCH1, notch homolog 1; TGF-α, transforming growth factor alpha; AMF, autocrine motility factor; CXCR4, fibronectin; MMPs, matrix metalloproteinases; uPAR, urokinase plasminogen receptor; CD44, cluster of differentiation 44; ABCG2, ATP-binding cassette sub-family G member 2; Oct3/4, octamer-binding transcription factor 4

identified as regulating the metabolic adaptation to acidosis whereas HIF-1α has been found to be downregulated with acidosis ([35] and the references therein). Hypoxia and acidosis have also been identified as playing a role in immune suppression ([37] and the references therein).

Different molecular and functional imaging techniques are available or are being developed to detect hypoxia in human cancers and in cancer models. Such techniques can be used to identify cancers that may benefit from targeting hypoxia and hypoxia related pathways for precision medicine. Imaging can provide new insights into the relationship between hypoxia, vascularization, metabolism, the ECM, stromal cells, invasion and metastasis. Such insights can advance understanding of the role of hypoxia in cancer progression, and identify therapeutic interventions to reduce cancer aggressiveness. Here we have presented an overview of the applications of molecular and functional imaging to detect hypoxia, and the insights that have been gained from the applications of imaging studies to understand the causes and the consequences of hypoxia in cancer. We have also presented new directions in exploiting hypoxia for theranostic imaging strategies.

2 Molecular and functional imaging techniques to detect hypoxia

Several noninvasive imaging modalities, many of which are clinically translatable, are currently available to detect hypoxia in tumors. While early studies with electrodes to detect hypoxia in cancers were valuable in demonstrating the presence of hypoxia in human cancers and animal models [38, 39], the drawbacks of electrode measurements included potential tissue damage, limited and highly localized sampling of tissue, and requirement of tumor accessibility to the electrodes. With noninvasive imaging, the entire tissue can be sampled, and depending upon the imaging modality and the technique used, both spatial and temporal information can be obtained from anywhere within the body. Techniques available to detect hypoxia can be broadly categorized based on the different imaging modalities such as positron imaging tomography (PET), magnetic resonance imaging (MRI/electron paramagnetic resonance imaging, EPRI), optical imaging (OI), and photoacoustic imaging (PAI). Advantages and limitations of these methods have been extensively reviewed [40–43].

2.1 PET imaging

Observations that ^{14}C-labeled derivatives of N-alkyl-2-nitroimidazoles were trapped in cells that were hypoxic [44–48] formed the basis of the development of 2-nitroimidazoles as hypoxia imaging agents using radioactive tracers. Currently, ^{18}F-fluromisonidazole (^{18}F-FMISO) is the most widely used PET tracer for detecting hypoxia in human studies. Its limitations are a spatial resolution of ~ 5 mm and slow uptake and washout kinetics [49]. This has led to the development of ^{18}F tracers such as ^{18}F-fluoroazomycin-arabinofuranoside (^{18}F-FAZA) that has improved tracer kinetics and higher hypoxia-based contrast [50]. ^{18}F-FAZA has been found to be useful in patient stratification and response evaluation to hypoxic cytotoxins in head and neck cancers [51]. Additional fluorine-based radiotracers from the nitroimidazole family that are currently being evaluated include ^{18}F-fluoroetanidazole (^{18}F-FETA), ^{18}F-2-nitroimidazol-pentafluoropropyl acetamide (^{18}F-EF5), ^{18}F-flortanidazole (^{18}F-XH4), and 1-(2-[^{18}F]-fluoro-1-[hydroxymethyl]ethoxy)methyl-2-nitroimidazole (^{18}F-RP-170) [50]. Other PET tracers include copper-labeled thiosemicarbazones such as ^{62}Cu-ATSM (copper diacetyl-bis(N^4-methylthiosemicarbazone)). Although the specificity of ^{62}Cu-ATSM to hypoxia has been demonstrated, one potential problem is that this may be cell-line specific [49]. Efforts are also being made to use the detection of CAIX that is upregulated with hypoxia as a marker of hypoxia using small molecules developed as CAIX inhibitors [49, 52]. These include novel sulfonamide-containing compounds, such as 2-[^{18}F]-3,5,6-trifluoro-3′-sulfamoylbenzanilide (^{18}F-TFSB), and a low molecular weight dual motif PET ligand [^{64}Cu]XYIMSR-06 targeting CAIX.

2.2 Magnetic resonance imaging

MRI methods such as oxygen-enhanced MRI (OE-MRI), also known as tumor oxygenation level-dependent (TOLD) MRI, and blood oxygenation level-dependent (BOLD) MRI detect hypoxia based on changes in water T_1 or T_2*, respectively [53]. In OE-MRI, oxygen breathing in combination with dynamic contrast-enhanced (DCE) MRI is used to identify hypoxic tumor regions based on changes in T_1. In BOLD MRI, differences in oxygenated and deoxygenated hemoglobin generate a signal that reflects blood oxygen saturation. However, to derive tissue oxygenation, knowledge of blood volume and oxygen consumption is required. Advantages of BOLD MRI include the use of intrinsic contrast that does not require injection of a contrast agent, and avoidance of the complications of radioactive tracers. BOLD MRI has been applied in several human tumor studies [54–57]. Significant changes in BOLD contrast were detected in head and neck cancer patients breathing hyperoxic gas [58]. BOLD response to breathing oxygen before chemotherapy was significantly different in tumors with good therapeutic outcome compared to those with poor response [59], whereas traditional DCE-MRI failed to identify differences. OE-MRI or TOLD contrast is also increasingly being used to detect oxygenation in preclinical [60, 61] and human studies [62–64].

Another approach to detect hypoxia with MR spectroscopic imaging (MRSI) is with the use of compounds such as perfluorocarbons or hexamethyldisoloxane (HMDSO) that have oxygen-dependent relaxivity. Oxygen tensions can be

determined from changes in relaxivity of perfluorcarbons (^{19}F MRSI) or HMDSO (^{1}H MRSI) obtained using spectroscopic MRI of the tumor following intratumoral injections [65, 66]. These approaches have been used to understand the role of hypoxia in resistance to radiation therapy in preclinical models [67] but have not been attempted in human studies.

2.3 Optical imaging

HRE-driven expression of luciferase or fluorescent proteins has been extensively used to detect biological hypoxia with bioluminescent imaging (luciferase) or optical imaging (green or red fluorescence protein), respectively [68–71]. The bioluminescence generated by the action of luciferase on the injected substrate, luciferin, requires ATP and O_2, but even under exceedingly low PO_2, there is sufficient oxygen to induce bioluminescence. Recently, an HRE-driven imaging strategy that combined the hypoxia-driven expression of two reporters, luciferase and enhanced green fluorescence protein (EGFP), that have significantly different half-lives was developed to detect temporal changes in hypoxia and HIF activity in tumors [72]. These HRE-driven systems are valuable in mechanistic studies designed to understand the relationship between hypoxia, acidic pH, the ECM, vascularization, and stromal cells but are not clinically translatable.

2.4 Photoacoustic imaging

PAI is a recently developed hybrid technology that has significant promise for several applications in cancer discovery and treatment [73]. Compared to optical imaging, PAI provides significantly higher resolution at imaging depths of up to 4 cm resulting in an improved translatable capability, when scaling from mice to humans. PAI combines the molecular sensitivity of optical imaging with the high-resolution (up to 100 times greater) and real-time aspects of ultrasound and overcomes the depth issues of strictly optical techniques. In PAI, a narrow-pulse-width laser is used to excite tissue, where it is absorbed and converted to heat, causing thermal expansion that, in turn, generates an acoustic signal that is measured with an ultrasound transducer. Hemoglobin in the blood is the dominant endogenous absorber of near-infrared (NIR) light. The oxygen saturation determines if hemoglobin is bound to oxygen (oxyhemoglobin, HbO_2) or unbound (deoxyhemoglobin, HHb). HbO_2 and HHb have characteristic absorption spectra that affect the PA signal at a given wavelength. After linear unmixing of the PA signal, the relative concentration of each hemoglobin type can be determined to derive blood oxygen saturation (SO_2) that reflects oxygenation. PAI devices are available for animal studies [73], with commercially available devices being developed for human applications [74–76].

3 Applications of imaging cancer hypoxia

3.1 Hypoxia targeting

The major applications of imaging in cancer hypoxia have been for the purpose of identifying patients who may benefit from hypoxia-targeted therapies. Hypoxia-targeted therapies include use of radiation sensitizers such as misonidazole, increasing oxygen delivery, decreasing oxygen consumption, using hypoxia-activated prodrugs, and radiation therapy dose-painting strategies to increase dose to hypoxic regions [77]. These hypoxia-targeted therapies have shown mixed responses. Theoretically, such therapies will only be effective if patients with hypoxic tumors are selected for treatment. For instance, it is likely that a set of trials with evofosfamide failed because patients with hypoxia were not stratified [78–80]. Using gene signatures associated with hypoxia in biopsy samples is one option being pursued to identify patients with hypoxic tumors [81–83]. However, such approaches only provide a "snap-shot" of a continually changing landscape. Imaging is therefore being integrated into many of the clinical trials incorporating these hypoxia-targeting strategies [84]. Some trials have confirmed that hypoxia predicted for locoregional failure [85], but many of these trials such as those for non-small cell lung cancer are still ongoing including radiation painting to boost radiation therapy in hypoxic tumor regions [84].

3.2 Hypoxia and vascularization

Since inadequate perfusion is a major cause of tumor hypoxia, establishing the relationship between tumor vascularization and hypoxia would allow the use of clinically translatable perfusion-based methods such as DCE-MRI to predict for hypoxia in tumors.

In a recent multiparametric MRI study of 20 patients with breast lesions, quantitative BOLD (qBOLD) and vascular architecture mapping (VAM), MRI biomarker maps of oxygen extraction fraction (OEF), metabolic rate of oxygen (MRO_2), and mitochondrial oxygen tension ($mitoPO_2$) were used to measure tissue hypoxia and neovascularization including vascular architecture parameters such as micro-vessel radius (VSI), density (MVD), and type (MTI). High OEF was associated with low MVD and *vice versa*, and MRO_2 values showed spatial congruence with VSI. Invasive ductal carcinomas were found to consume more oxygen and were more hypoxic and neovascularized than benign tumors [86].

A relationship between DCE-MRI and hypoxia, detected by pimonidazole staining, was also observed in untreated and sunitinib-treated pancreatic ductal adenocarcinoma (PDAC) xenografts. Results from these studies suggest that K^{trans} (volume transfer constant) obtained from DCE-MRI may provide an index of tumor vascular density and hypoxia in untreated as well

as sunitinib-treated PDACs [87]. Using PAI, together with an oxygen gas challenge to visualize the spatiotemporal heterogeneity of tumor vascular function, oxygenation dynamics were found to be significantly different in prostate cancer models with markedly different vascular function [88]. In another study, combined vascular DCE-MRI and optical imaging was performed to understand the relationship between hypoxia and vascularization in a human prostate cancer model engineered to express EGFP under hypoxia. MRI measurements showed that vascular volume was significantly lower in fluorescing regions (Fig. 2a). These regions also frequently exhibited high permeability. These observations are consistent with the possibility that regions of low vascular volumes are hypoxic, which induces increased expression of functionally active VEGF, a potent vascular permeability factor [70].

However, in a study with glioblastoma multiforme (GBM), tumors with higher uptake of ^{18}F-FMISO also showed higher cerebral blood volume (CBV), suggesting that tumor hypervascularization in GBM, as assessed by the CBV on MRI, did not result in effective tissue oxygenation [92]. Oxygen consumption will also affect tissue oxygenation that may explain the results observed here. As multiplexed PET-MR scanners become increasingly available for preclinical and human studies, these combined approaches of using

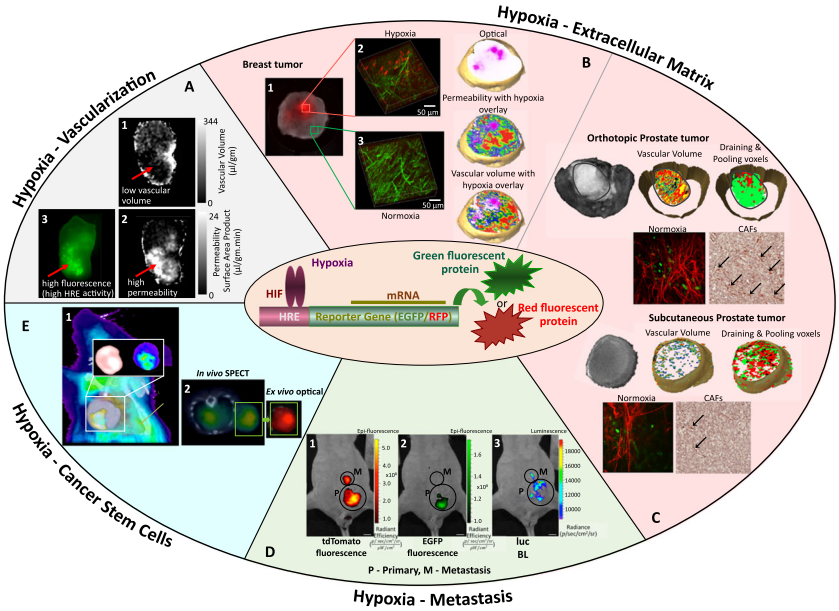

Fig. 2 Examples of the applications of imaging to understand the relationship between hypoxia and vascularization, hypoxia and the ECM, hypoxia and metastasis, and hypoxia and cancer stem cells. (A) Representative maps of (1) vascular volume (VV), and (2) permeability surface area product (PS) MRI parameters obtained from the central slice of an HRE-EGFP PC-3 tumor (180 mm^3). VV ranged from 0 to 344 μL/g and PS from 0 to 24 μL/g min. (3) Fluorescent microscopy image of a fresh tissue slice obtained from the MR-imaged slice, obtained using a Nikon TS100-F microscope (1× objective) with a wavelength of 512 nm. Co-localization is observed between the fluorescing hypoxic tumor region in the optical image and regions of low vascular volume and higher permeability in the MRI images. Adapted from [70]. (B) (1) *Ex vivo* 1× bright field and overlaid fluorescence image showing the location of hypoxic regions on the tumor section. 3D visualization of Col1 fibers in (2) hypoxic and (3) normoxic fields of view. Hypoxic regions are displayed in red and Col1 fibers in green. On the right are displayed 3D reconstructed images of a representative tumor with hypoxic regions displayed in pink (top), and an overlay of the hypoxia mask on the vascular volume map (middle), and permeability map (bottom). Fewer Col1 fibers and macromolecular transport are detected in hypoxic tumor regions. Adapted from [89]. (C) Representative anatomic and functional images of an orthotopic and a subcutaneous PC3-HRE-EGFP tumor. The orthotopic tumor is delineated by a white line in the anatomic image. Representative maps of vascular volume and draining (red) and pooling (green) voxels from the orthotopic tumor (top) and subcutaneous tumor (bottom) are shown together with representative images of Col1 fibers (red) overlaid with EGFP expression (green), and α-SMA-immunostained sections showing the presence of CAFs marked by arrows. More Col1 fibers and CAFs are detected in metastatic orthotopic tumors compared to nonmetastatic subcutaneous tumors. Adapted from [90]. (D) Representative *in vivo* images from an orthotopic and subcutaneous PC3-HRE-EGFP/HRE-ODD-luc/tdTomato tumor with a peritoneal metastatic lesion revealing patterns of green fluorescence protein (EGFP) and bioluminescence (luc) expression in primary and metastatic lesions. Optical images are from (1) tdTomato expression to identify cancer cells, (2) HRE-driven EGFP expression, and (3) HRE-driven luc expression. Scale bar 0.5 cm. The primary tumor had a focus of EGFP expression indicative of long-term exposure to hypoxia that was also identified with bioluminescent imaging but with a smaller area, suggesting that the hypoxia may have been resolving. In contrast, there was an extensive area of BL in the primary and as well as the metastatic lesion that was not identified in the EGFP image that suggested that this region was newly hypoxic. Adapted from [91]. (E) (1) *In vivo* co-registration of RFP expression from optical images (blue), and SPECT images (yellow) showing the overlap of a hypoxic region of high fluorescence with high CD44 antibody localization. Inset shows *ex vivo* SPECT (left) and optical (right) images of a fresh 2-mm slice from the tumor. (2) *In vivo* SPECT imaging of a SCID mouse bearing MDA-MB-231-HRE-tdTomato RFP tumor was performed in 64 projections at 30 s/projection. A representative transaxial slice of decay-corrected, volume-rendered SPECT/CT images at 48 h demonstrate a region of high intensity that co-localized with a red fluorescing hypoxic tumor region in the corresponding *ex vivo* optical image. Adapted from [71]

PET imaging for hypoxia and DCE-MRI to map vascular parameters will provide additional insights into the evolution of hypoxia in tumors, and the vascular characteristics that drive the formation of hypoxia in cancers.

3.3 Hypoxia, metabolism, the ECM, invasion and, metastasis

Imaging has been applied to understand the relationship between hypoxia, metabolism, the ECM, invasion, and metastasis in studies using intact perfused cells in microfluidic devices or cell perfusion systems that allow carefully controlled regulation of oxygen tensions, and in human tumor xenografts. Examples of imaging applications to understand the relationship between hypoxia and vascularization, the ECM, macromolecular transport, CD44 expression, and detecting patterns of hypoxia and reoxygenation in metastatic and nonmetastatic tumors are presented in Fig. 2a–e.

3.3.1 Metabolism

In a recent MRS and multiphoton optical imaging study, a microfluidic model that recapitulated the ductal carcinoma *in situ* (DCIS) microenvironment was developed to understand the development of hypoxia in DCIS. A DCIS cell line was grown inside a luminal mammary duct model, embedded in a 3D hydrogel with mammary fibroblasts in the microdevice. Hypoxia and nutrient starvation were detected in the DCIS resulting in an altered metabolism of glycolysis and other hypoxia-associated pathways that were in good agreement with patient genomic profiles. Additionally, the hypoxia-activated prodrug tirapazamine selectively destroyed hypoxic DCIS cells [93].

In an intact cell perfusion study, triple (estrogen receptor/progesterone receptor/HER2neu) negative, invasive MDA-MB-231 and SUM149 human breast cancer cells were engineered to silence the expression of HIF-1α, HIF-2α, or both isoforms of HIF-α. An imaging compatible cell perfusion system was used to determine the effects of HIF silencing on metabolism and invasion under carefully controlled normoxic and hypoxic conditions [94]. HIF-2α played a major role in altering cell metabolism. Lipids and lipid droplets were significantly reduced in HIF-2α and double silenced MDA-MB-231 and SUM149 cells, implicating HIF in their regulation [94]. In addition, lactate production and glucose consumption were reduced. Metabolic changes detected in the intact cell perfusion system were also identified in solid tumors derived from these cells, using noninvasive metabolic imaging and high-resolution ^{1}H MRS of tumor extracts [95]. These imaging studies identified new metabolic targets of HIF and demonstrated the divergent consequences of silencing HIF-1α and HIF-2α individually on some of these targets. Such studies expand our understanding of the metabolic pathways regulated by HIFs and the adaptive metabolic response of cancer cells to hypoxia that may lead to novel metabolism-based therapeutic targets for triple negative breast cancer.

3.3.2 ECM, invasion, and metastasis

The tumor ECM contains proteoglycans and fibrous protein such as collagen, elastin, fibronectin, and laminin [96]. HIFs transcriptionally regulate several genes and pathways that shape the ECM to facilitate invasion and metastasis [30, 31, 97–101]. Various isoforms of matrix metalloproteinases (MMPs), urokinase plasminogen activator (uPA) and its receptor, cathepsin D, tissue inhibitors of metalloproteinases (TIMPs), and lysyl oxidase (LOX) are hypoxia-inducible and regulated by HIF [99, 102]. Applications of noninvasive imaging using intact cell systems avoid the complexities of *in vivo* tumors with careful control of oxygen tensions [94], without changes in pH or substrate delivery that typically accompany the inadequate vascularization that causes hypoxia. Studies with an imaging-compatible cell perfusion that quantifies invasion over time revealed that silencing HIF-1α alone was not sufficient to attenuate invasiveness in MDA-MB-231 and SUM149 cancer cells. A significant reduction of metastatic burden was observed in single (HIF-1α or HIF-2α) and double α-isoform-silenced cells. This reduction was most evident when both HIF-1α and HIF-2α were silenced, suggesting that *in vivo*, cells in or near hypoxic regions are likely to be more invasive. The data also suggested that targeting HIF-1α alone was not sufficient to attenuate invasiveness, and that both HIF-1α and HIF-2α played a role in the metastatic cascade [94].

In an *in vivo* optical imaging study, a novel fluorescent mCherry hypoxia-responsive marker was used in real-time imaging to specifically and sensitively identify hypoxic cells at single-cell resolution. Hypoxic MDA-MB-231 cells showed a more persistent slow migration phenotype with abundant invadopodia, as compared to normoxic cells in the same field *in vivo*, and moved to congregate near flowing blood vessels. Cell populations that migrated toward human epithelial growth factor gradients *in vivo* were enriched with hypoxic cancer cells with increased collagen degradation and intravasation activity, characteristic of dissemination, and metastasis competent tumor cells [103].

The relationship between hypoxia, collagen 1 (Col1) fibers, and macromolecular transport was also investigated with molecular and functional imaging of the MDA-MB-231 tumor model [89]. The influence of hypoxia on macromolecular transport in tumors, and the role of Col1 fibers in mediating this transport were investigated using an MDA-MB-231 breast cancer xenograft model engineered to express red fluorescent protein under hypoxia. MRI of macromolecular transport was combined with second harmonic generation (SHG)

microscopy of Col1 fibers. Consistent with the increased collagen degradation reported earlier [103], hypoxic tumor regions displayed significantly decreased Col1 fiber density and volume, as well as significantly lower macromolecular draining and pooling rates, than normoxic regions. Results from these studies suggest that Col1 fibers may facilitate macromolecular transport in tumors, and their reduction in hypoxic regions may reduce this transport. Reduction of macromolecular transport in hypoxic regions may also contribute to poor drug delivery. These studies also reported higher Col1 fiber density around hypoxic regions that may facilitate the escape of aggressive hypoxic cancer cells along aligned Col1 fiber tracks [104].

In a separate study identifying the role of HIFs in modifying the ECM and the tumor microenvironment (TME), tumors derived from MDA-MB-231 cells with HIF-1α or HIF-2α or both HIF-1α and HIF-2α silenced contained higher percent fiber volume and lower interfiber distance, as detected by SHG microscopy, compared to tumors derived from empty vector MDA-MB-231 cells, together with changes in Col1-degrading enzymes, and enzymes involved in Col1 synthesis and deposition [31]. A reduction in LOX protein expression in HIF-down-regulated tumors suggested that more non-cross-linked fibers were present [31].

Patterns of hypoxia in the primary tumor and metastatic environments of a human prostate cancer were recently investigated using an imaging strategy based on the HRE-driven expression of long-lived EGFP and short-lived luciferase (luc) fused to the oxygen-dependent degradation (ODD) domain in prostate cancer PC-3 cells [91]. This "timer" strategy was used to provide information on the temporal evolution of HIF activity and hypoxia in metastatic PC-3 tumors implanted orthotopically in the prostate and non-metastatic PC-3 tumors implanted subcutaneously. By combining long-lived EGFP and a short-lived luc, identification of normoxic (EGFP−/luc−), hypoxic (EGFP+/luc+) or (EGFP−/luc+), and reoxygenated (EGFP+/luc−) tumor microenvironments was possible. Results from these studies suggested that hypoxia followed by reoxygenation may result in a more metastatic phenotype, and that hypoxia alone was not sufficient to permit metastasis.

An additional role of hypoxia in cancer aggression includes regulation of CD44, a transmembrane glycoprotein that plays multifaceted roles in tumor progression and metastasis and is associated with a stem-like phenotype in many cancers [105]. *In vivo* imaging studies with tumor xenografts derived from MDA-MD-231 cells engineered to express HRE-driven tdTomato red fluorescence protein expression identified co-localization between hypoxic fluorescent regions and high CD44 expressing regions identified by ^{125}I-radiolabeled CD44 antibody [71].

In studies of GBM [106], the invasive margin was defined by the region with 5-aminolevulinic acid (GliolanTM) fluorescence at surgery beyond the T_1 enhancing region on MRI. Aldehyde dehydrogenase 1 (ALDH1) and Nestin immunohistochemistry were used as a measure of stem-like properties. Analysis of the core, rim, and invasive regions showed significantly increased fibroblast growth factor (FGF) and ALDH1 expression and decreased Nestin expression in the invasive zone, with elevated HIF-1α in the rim region, adjacent to the hypoxic core. These studies highlight the heterogeneity in tumors and the distinct molecular composition of the heterogeneous invasive margin compared to the tumor core and the importance of sampling the invasive margin compared to the tumor core when developing targeted agents for residual GBM.

Another mechanism by which hypoxia can regulate cancer aggression includes modification of pHe. CAIX, a hypoxia-inducible tumor-associated cell surface enzyme, is thought to acidify the TME by hydrating CO_2 to form protons and bicarbonate. Cancer cells can also trigger activation of CAIX on cancer-associated fibroblasts (CAFs) to help increase extracellular acidification [107, 108]. CAIX on CAFs has been shown to promote cancer progression by driving the epithelial-mesenchymal transition and is a better predictor of treatment outcome compared to CAIX expressed by cancer cells [109]. CAIX detected on CAFs in hypoxic environments in lung adenocarcinoma contributed to a more aggressive phenotype [110].

In a recent ^{1}H MRS imaging study, CAIX-expressing tumors had 0.15 pH-unit lower median pHe than control tumors, suggesting that CAIX maintains an acidic tumor pHe that is tolerated by cancer cells and favors invasion and metastasis [111]. In another recent study with amide proton transfer MRI that provides a pH-dependent signal, a reduction of tumor hypoxia was associated with a shift in tumor pH [112].

4 Theranostic strategies exploiting hypoxia

Theranostics is a recent, largely nanomedicine-driven, field at the interface of diagnosis and therapy that holds significant promise for precision medicine of cancer [113]. In theranostic strategies, detection and imaging are combined to visualize the delivery of therapy to the target of interest in an effort to induce minimal toxicity in normal tissues (Fig. 3). Radiation therapy dose painting, where a boost of radiation is delivered to hypoxic tumor regions, identified by imaging, is one example of hypoxia theranostics. However, increasingly, there is a trend to develop novel nanoparticles (NPs), or targeted small molecules with α- or β-emitters for hypoxia-based radiotheranostics [114].

There is a major effort to target hypoxia by using CAIX-binding agents since CAIX is expressed by hypoxic cells [115]. By using a low molecular weight bivalent ureidosulfonamide scaffold that binds to CAIX, complexed with ^{111}In for single-photon emission computed tomography (SPECT) imaging to detect CAIX, and ^{90}Y for radionuclide therapy, significantly delayed HT-29 tumor growth was observed [116]. Hypoxia-targeted gold nanorods (GNRs)

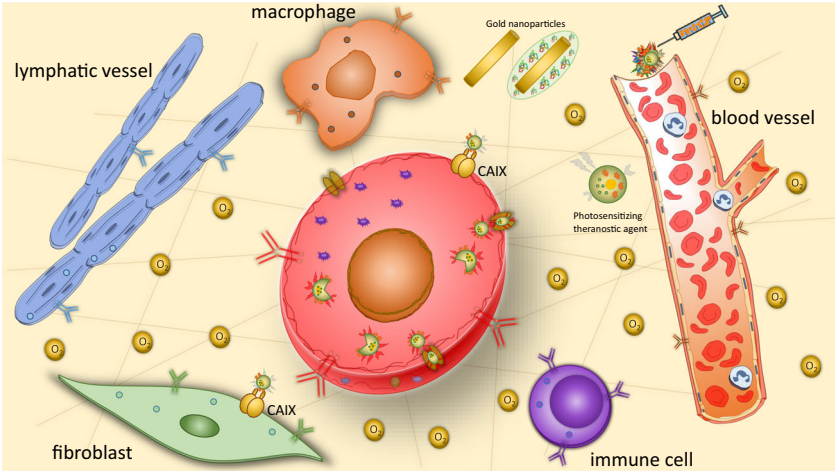

Fig. 3 Schematic representing the concept of hypoxia-targeted theranostic strategies. Displayed in the schematic are NPs targeting CAIX and hypoxic tumor microenvironments. Adapted from [113]

conjugated to a CAIX antibody for cancer photothermal therapy were recently described [117]. *In vivo* biodistribution was performed with hyperspectral imaging, and NIR ablation using the GNRs eliminated CAIX expressing cells in tumors that showed regression following treatment. Other CAIX-binding approaches include using a "click-chemistry" approach to deliver an apoptosis inducer [118].

In another approach, a molecular probe, IR1048-MZ, was synthesized by conjugating a nitro imidazole group as a hypoxia-specific trigger with IR1018 as a NIR/PA signal reporter for PAI and photothermal therapy [119]. An additional strategy for hypoxia targeting includes delivery of hypoxia-responsive lipid-poly-(hypoxic radiosensitized polyprodrug) NPs that were tested in a glioma model [120]. Theranostic liposomes with the hypoxia activatable prodrug AQ4N showed toxicity only in the hypoxic region of 4T1 breast tumors [121]; *ex vivo* immunofluorescence staining with pimonidazole was used to confirm hypoxia status.

The availability of NPs to deliver cDNA [122] creates the possibility of delivering cDNA coding for HRE-driven prodrug enzyme expression, to specifically target hypoxic cells. Advances in HRE-driven expression of prodrug/suicide gene enzymes thymidine kinase (TK) and cytosine deaminase (CD) were demonstrated by hypoxia-driven expression of the triple suicide gene TK/CD/UPRT expression that enhanced cytotoxicity to ganciclovir (GCV) and 5-fluorocytosine (5-FC) and sensitized human colorectal HCT8 cancer cells to radiation *in vitro* and *in vivo* [123]. HCT8 cells expressing hypoxia-inducible vectors (HRE-TK/eGFP and HRE-CD/UPRT/mDsRed) were established. The distribution of TK/eGFP and CD/UPRT/mDsRed expression, visualized with fluorescence microscopy, co-localized with the hypoxia marker pimonidazole-positive staining cells. Administration of 5-FC and GCV in mice in combination with local irradiation resulted in tumor regression, as compared with prodrug or radiation treatments alone.

While all of the hypoxia-based theranostic strategies are currently in the discovery stage, the CAIX-targeted radiotheranostic strategies have the possibility of rapid translation, whereas the NPs have a higher barrier to clear for translation. Since most of the NPs are cleared through organs such as the liver and spleen, toxicity should be carefully evaluated. Future hypoxia-targeting studies should also evaluate if extracellular acidosis is reversed with treatment, and if the effects of extracellular acidosis on invasion and metastasis are attenuated.

5 Conclusions

While considerable advances have been made in the applications of imaging to understand the causes and consequences of hypoxia in cancers, several areas are still relatively unexplored, especially within the context of invasion and metastasis. Recent advances in immune checkpoint inhibitors and their success in some cancers but not in others highlight the importance of imaging programmed death-ligand 1 (PD-L1)/programmed cell death protein 1 (PD-1) expression within the complex TME to understand the role of hypoxia, acidic pH, vascularization, metabolism, and the ECM in immune cell trafficking and immune checkpoint expression. Similarly, CAFs play an important role in several aspects of cancer aggression [90, 124–126]. The ability to dynamically image CAF trafficking within the context of hypoxia, acidic pH, and the TME would advance our understanding of the role of hypoxia and CAFs in cancer invasion and metastasis.

Another area where imaging can contribute significantly is in understanding the premetastatic niche and the role of hypoxia in establishing the premetastatic niche. Recent studies have used label-free Raman spectroscopy to detect stromal changes in the premetastatic lung niche in a breast cancer model [127].

The development of artificial intelligence algorithms to identify aggressive habitats in cancers from radiogenomics data [128] will provide new approaches to understand and exploit hypoxia in cancers for detection and treatment.

Lastly, little is known about the mechanical cues that make cancer cells migrate [129–131]. Applications of molecular and functional imaging techniques to investigate *in vivo* mechanotransduction pathways such as those mediated by focal adhesion kinase (FAK) [132, 133] within hypoxic and acidic environments are unexplored. Future imaging studies that investigate mechanotransduction pathways through FAK or other molecular pathways imaging to visualize mechanotransduction responses to Col1 fiber patterns, oxygenation, and CAF trafficking will provide a unique window into a critical element of the metastatic cascade.

Acknowledgments We gratefully acknowledge valuable discussions with Dr. R. J. Gillies over the past two decades.

Funding information Support from NIH R01 CA82337, R01 CA136576, R01 CA193365, and R35 CA209960 is gratefully acknowledged.

Publisher's note Springer Nature remains neutral with regard to jurisdictional claims in published maps and institutional affiliations.

References

1. Dunwoodie, S. L. (2009). The role of hypoxia in development of the mammalian embryo. *Developmental Cell, 17*(6), 755–773. https://doi.org/10.1016/j.devcel.2009.11.008.
2. Giordano, F. J. (2005). Oxygen, oxidative stress, hypoxia, and heart failure. *The Journal of Clinical Investigation, 115*(3), 500–508. https://doi.org/10.1172/JCI24408.
3. Nathan, S. D., Barbera, J. A., Gaine, S. P., Harari, S., Martinez, F. J., Olschewski, H., Olsson, K. M., Peacock, A. J., Pepke-Zaba, J., Provencher, S., Weissmann, N., & Seeger, W. (2018). Pulmonary hypertension in chronic lung disease and hypoxia. *The European Respiratory Journal, 53*, 1801914. https://doi.org/10.1183/13993003.01914-2018.
4. Hong, W. X., Hu, M. S., Esquivel, M., Liang, G. Y., Rennert, R. C., McArdle, A., Paik, K. J., Duscher, D., Gurtner, G. C., Lorenz, H. P., & Longaker, M. T. (2014). The role of hypoxia-inducible factor in wound healing. *Advances Wound Care (New Rochelle), 3*(5), 390–399. https://doi.org/10.1089/wound.2013.0520.
5. Maxwell, P. H., Dachs, G. U., Gleadle, J. M., Nicholls, L. G., Harris, A. L., Stratford, I. J., Hankinson, O., Pugh, C. W., & Ratcliffe, P. J. (1997). Hypoxia-inducible factor-1 modulates gene expression in solid tumors and influences both angiogenesis and tumor growth. *Proceedings of the National Academy of Sciences of the United States of America, 94*(15), 8104–8109.
6. Horsman, M. R., Mortensen, L. S., Petersen, J. B., Busk, M., & Overgaard, J. (2012). Imaging hypoxia to improve radiotherapy outcome. *Nature Reviews. Clinical Oncology, 9*(12), 674–687. https://doi.org/10.1038/nrclinonc.2012.171.
7. Gillies, R. J., Brown, J. S., Anderson, A. R. A., & Gatenby, R. A. (2018). Eco-evolutionary causes and consequences of temporal changes in intratumoural blood flow. [review]. *Nature Reviews. Cancer, 18*(9), 576–585. https://doi.org/10.1038/s41568-018-0030-7.
8. Unwith, S., Zhao, H., Hennah, L., & Ma, D. (2015). The potential role of HIF on tumour progression and dissemination. *International Journal of Cancer, 136*(11), 2491–2503. https://doi.org/10.1002/ijc.28889.
9. Vaupel, P., Kelleher, D. K., & Thews, O. (1998). Modulation of tumor oxygenation. *International Journal of Radiation Oncology, Biology, Physics, 42*(4), 843–848.
10. Danhier, F., Danhier, P., Magotteaux, N., De Preter, G., Ucakar, B., Karroum, O., et al. (2012). Electron paramagnetic resonance highlights that the oxygen effect contributes to the radiosensitizing effect of paclitaxel. *PLoS One, 7*(7), e40772. https://doi.org/10.1371/journal.pone.0040772.
11. Toma-Dasu, I., & Dasu, A. (2013). Modelling tumour oxygenation, reoxygenation and implications on treatment outcome. *Computational and Mathematical Methods in Medicine, 2013*, 141087–141089. https://doi.org/10.1155/2013/141087.
12. White, D. A., Zhang, Z., Li, L., Gerberich, J., Stojadinovic, S., Peschke, P., & Mason, R. P. (2016). Developing oxygen-enhanced magnetic resonance imaging as a prognostic biomarker of radiation response. *Cancer Letters, 380*(1), 69–77. https://doi.org/10.1016/j.canlet.2016.06.003.
13. Semenza, G. L., & Wang, G. L. (1992). A nuclear factor induced by hypoxia via *de novo* protein synthesis binds to the human erythropoietin gene enhancer at a site required for transcriptional activation. *Molecular and Cellular Biology, 12*(12), 5447–5454.
14. Wang, G. L., Jiang, B. H., Rue, E. A., & Semenza, G. L. (1995). Hypoxia-inducible factor 1 is a basic-helix-loop-helix-PAS heterodimer regulated by cellular O2 tension. *Proceedings of the National Academy of Sciences of the United States of America, 92*(12), 5510–5514.
15. Kaelin, W. G., Jr., & Ratcliffe, P. J. (2008). Oxygen sensing by metazoans: The central role of the HIF hydroxylase pathway. *Molecular Cell, 30*(4), 393–402. https://doi.org/10.1016/j.molcel.2008.04.009.
16. Epstein, A. C., Gleadle, J. M., McNeill, L. A., Hewitson, K. S., O'Rourke, J., Mole, D. R., et al. (2001). C. elegans EGL-9 and mammalian homologs define a family of dioxygenases that regulate HIF by prolyl hydroxylation. *Cell, 107*(1), 43–54.
17. Semenza, G. L., Jiang, B. H., Leung, S. W., Passantino, R., Concordet, J. P., Maire, P., & Giallongo, A. (1996). Hypoxia response elements in the aldolase A, enolase 1, and lactate dehydrogenase A gene promoters contain essential binding sites for hypoxia-inducible factor 1. *The Journal of Biological Chemistry, 271*(51), 32529–32537.
18. Tanaka, T., Wiesener, M., Bernhardt, W., Eckardt, K. U., & Warnecke, C. (2009). The human HIF (hypoxia-inducible factor)-3 alpha gene is a HIF-1 target gene and may modulate hypoxic gene induction. *Biochemical Journal, 424*, 143–151. https://doi.org/10.1042/Bj20090120.
19. Koh, M. Y., & Powis, G. (2012). Passing the baton: The HIF switch. *Trends in Biochemical Sciences, 37*(9), 364–372. https://doi.org/10.1016/j.tibs.2012.06.004.
20. Nakazawa, M. S., Keith, B., & Simon, M. C. (2016). Oxygen availability and metabolic adaptations. *Nature Reviews. Cancer, 16*(10), 663–673. https://doi.org/10.1038/nrc.2016.84.
21. Carmeliet, P., Dor, Y., Herbert, J. M., Fukumura, D., Brusselmans, K., Dewerchin, M., Neeman, M., Bono, F., Abramovitch, R., Maxwell, P., Koch, C. J., Ratcliffe, P., Moons, L., Jain, R. K., Collen, D., & Keshet, E. (1998). Role of HIF-1alpha in hypoxia-mediated apoptosis, cell proliferation and tumour angiogenesis. *Nature, 394*(6692), 485–490. https://doi.org/10.1038/28867.
22. Semenza, G. L. (2003). Targeting HIF-1 for cancer therapy. *Nature Reviews. Cancer, 3*(10), 721–732. https://doi.org/10.1038/nrc1187.
23. Zhong, H., Chiles, K., Feldser, D., Laughner, E., Hanrahan, C., Georgescu, M. M., Simons, J. W., & Semenza, G. L. (2000).

Modulation of hypoxia-inducible factor 1alpha expression by the epidermal growth factor/phosphatidylinositol 3-kinase/PTEN/AKT/FRAP pathway in human prostate cancer cells: Implications for tumor angiogenesis and therapeutics. *Cancer Research, 60*(6), 1541–1545.

24. Ivan, M., Kondo, K., Yang, H., Kim, W., Valiando, J., Ohh, M., Salic, A., Asara, J. M., Lane, W. S., & Kaelin, W. G. (2001). HIFalpha targeted for VHL-mediated destruction by proline hydroxylation: Implications for O2 sensing. *Science, 292*(5516), 464–468. https://doi.org/10.1126/science.1059817.
25. Maxwell, P. H., Wiesener, M. S., Chang, G. W., Clifford, S. C., Vaux, E. C., Cockman, M. E., Wykoff, C. C., Pugh, C. W., Maher, E. R., & Ratcliffe, P. J. (1999). The tumour suppressor protein VHL targets hypoxia-inducible factors for oxygen-dependent proteolysis. *Nature, 399*(6733), 271–275. https://doi.org/10.1038/20459.
26. Hudson, C. C., Liu, M., Chiang, G. G., Otterness, D. M., Loomis, D. C., Kaper, F., Giaccia, A. J., & Abraham, R. T. (2002). Regulation of hypoxia-inducible factor 1alpha expression and function by the mammalian target of rapamycin. *Molecular and Cellular Biology, 22*(20), 7004–7014.
27. Watson, J. A., Watson, C. J., McCann, A., & Baugh, J. (2010). Epigenetics, the epicenter of the hypoxic response. *Epigenetics, 5*(4), 293–296.
28. Iommarini, L., Porcelli, A. M., Gasparre, G., & Kurelac, I. (2017). Non-canonical mechanisms regulating hypoxia-inducible factor 1 alpha in cancer. *Frontiers in Oncology, 7*, 286. https://doi.org/10.3389/fonc.2017.00286.
29. Semenza, G. L. (2010). Defining the role of hypoxia-inducible factor 1 in cancer biology and therapeutics. *Oncogene, 29*(5), 625–634. https://doi.org/10.1038/onc.2009.441.
30. Gilkes, D. M., Semenza, G. L., & Wirtz, D. (2014). Hypoxia and the extracellular matrix: Drivers of tumour metastasis. *Nature Reviews. Cancer, 14*(6), 430–439. https://doi.org/10.1038/nrc3726.
31. Goggins, E., Kakkad, S., Mironchik, Y., Jacob, D., Wildes, F., Krishnamachary, B., & Bhujwalla, Z. M. (2018). Hypoxia inducible factors modify collagen I fibers in MDA-MB-231 triple negative breast cancer xenografts. *Neoplasia, 20*(2), 131–139. https://doi.org/10.1016/j.neo.2017.11.010.
32. Kakkad, S. M., Solaiyappan, M., O'Rourke, B., Stasinopoulos, I., Ackerstaff, E., Raman, V., et al. (2010). Hypoxic tumor microenvironments reduce collagen I fiber density. *Neoplasia, 12*(8), 608–617.
33. Penet, M. F., Chen, Z., & Bhujwalla, Z. M. (2011). MRI of metastasis-permissive microenvironments. *Future Oncology, 7*(11), 1269–1284. https://doi.org/10.2217/fon.11.114.
34. Gray, L. H., Conger, A. D., Ebert, M., Hornsey, S., & Scott, O. C. A. (1953). The concentration of oxygen dissolved in tissues at the time of irradiation as a factor in radiotherapy. *British Journal of Radiology, 26*(312), 638–648. https://doi.org/10.1259/0007-1285-26-312-638.
35. Corbet, C., & Feron, O. (2017). Tumour acidosis: From the passenger to the driver's seat. *Nature Reviews. Cancer, 17*(10), 577–593. https://doi.org/10.1038/nrc.2017.77.
36. Thews, O., & Riemann, A. (2019). Tumor pH and metastasis: A malignant process beyond hypoxia. *Cancer Metastasis Reviews*. https://doi.org/10.1007/s10555-018-09777-y.
37. Damgaci, S., Ibrahim-Hashim, A., Enriquez-Navas, P. M., Pilon-Thomas, S., Guvenis, A., & Gillies, R. J. (2018). Hypoxia and acidosis: Immune suppressors and therapeutic targets. *Immunology, 154*(3), 354–362. https://doi.org/10.1111/imm.12917.
38. Vaupel, P., Hockel, M., & Mayer, A. (2007). Detection and characterization of tumor hypoxia using pO(2) histography. *Antioxidants & Redox Signaling, 9*(8), 1221–1235. https://doi.org/10.1089/ars.2007.1628.
39. Stone, H. B., Brown, J. M., Phillips, T. L., & Sutherland, R. M. (1993). Oxygen in human tumors - correlations between methods of measurement and response to therapy - summary of a workshop held November 19-20, 1992, at the National-Cancer-Institute, Bethesda, Maryland. *Radiation Research, 136*(3), 422–434. https://doi.org/10.2307/3578556.
40. Challapalli, A., Carroll, L., & Aboagye, E. O. (2017). Molecular mechanisms of hypoxia in cancer. *Clinical and Translational Imaging, 5*(3), 225–253. https://doi.org/10.1007/s40336-017-0231-1.
41. Colliez, F., Gallez, B., & Jordan, B. F. (2017). Assessing tumor oxygenation for predicting outcome in radiation oncology: A review of studies correlating tumor hypoxic status and outcome in the preclinical and clinical settings. *Frontiers in Oncology, 7*, 10. https://doi.org/10.3389/Fonc.2017.00010.
42. Zhou, H. L., Arias-Ramos, N., Lopez-Larrubia, P., Mason, R. P., Cerdan, S., & Pacheco-Torres, J. (2018). Oxygenation imaging by nuclear magnetic resonance methods. *Preclinical Mri: Methods and Protocols, 1718*, 297–313. https://doi.org/10.1007/978-1-4939-7531-0_18.
43. Krohn, K. A., Link, J. M., & Mason, R. P. (2008). Molecular imaging of hypoxia. *Journal of Nuclear Medicine, 49*(Suppl 2), 129S–148S. https://doi.org/10.2967/jnumed.107.045914.
44. Chapman, J. D. (1979). Current concepts in cancer - hypoxic sensitizers - implications for radiation-therapy. *New England Journal of Medicine, 301*(26), 1429–1432. https://doi.org/10.1056/Nejm197912273012606.
45. Chapman, J. D., Franko, A. J., & Sharplin, J. (1981). A marker for hypoxic cells in tumors with potential clinical applicability. *British Journal of Cancer, 43*(4), 546–550. https://doi.org/10.1038/Bjc.1981.79.
46. Chapman, J. D. (1984). The detection and measurement of hypoxic cells in solid tumors. *Cancer, 54*(11), 2441–2449. https://doi.org/10.1002/1097-0142(19841201)54:11<2441::Aid-Cncr2820541122>3.0.Co;2-S.
47. Blasberg, R., Horowitz, M., Strong, J., Molnar, P., Patlak, C., Owens, E., & Fenstermacher, J. (1985). Regional measurements of [C-14] misonidazole distribution and blood-flow in subcutaneous Rt-9 experimental-tumors. *Cancer Research, 45*(4), 1692–1701.
48. Rasey, J. S., Grunbaum, Z., Magee, S., Nelson, N. J., Olive, P. L., Durand, R. E., et al. (1987). Characterization of radiolabeled fluoromisonidazole as a probe for hypoxic cells. *Radiation Research, 111*(2), 292–304. https://doi.org/10.2307/3576986.
49. Bonnitcha, P., Grieve, S., & Figtree, G. (2018). Clinical imaging of hypoxia: Current status and future directions. *Free Radical Biology and Medicine, 126*, 296–312. https://doi.org/10.1016/j.freeradbiomed.2018.08.019.
50. Marcu, L. G., Moghaddasi, L., & Bezak, E. (2018). Imaging of tumor characteristics and molecular pathways with PET: Developments over the last decade toward personalized cancer therapy. *International Journal of Radiation Oncology Biology Physics, 102*(4), 1165–1182. https://doi.org/10.1016/j.ijrobp.2018.04.055.
51. Graves, E. E., Hicks, R. J., Binns, D., Bressel, M., Le, Q. T., Peters, L., et al. (2016). Quantitative and qualitative analysis of [(18)F]FDG and [(18)F]FAZA positron emission tomography of head and neck cancers and associations with HPV status and treatment outcome. *European Journal of Nuclear Medicine and Molecular Imaging, 43*(4), 617–625. https://doi.org/10.1007/s00259-015-3247-7.
52. Minn, I., Koo, S. M., Lee, H. S., Brummet, M., Rowe, S. P., Gorin, M. A., et al. (2016). [64Cu]XYIMSR-06: A dual-motif CAIX ligand for PET imaging of clear cell renal cell carcinoma. *Oncotarget, 7*(35), 56471–56479. https://doi.org/10.18632/oncotarget.10602.
53. O'Connor, J. P. B., Robinson, S. P., & Waterton, J. C. (2019). Imaging tumour hypoxia with oxygen-enhanced MRI and

BOLD MRI. *The British Journal of Radiology*, 20180642. https://doi.org/10.1259/bjr.20180642.

54. Taylor, N. J., Baddeley, H., Goodchild, K. A., Powell, M. E., Thoumine, M., Culver, L. A., et al. (2001). BOLD MRI of human tumor oxygenation during carbogen breathing. [Research Support, Non-U.S. Gov't]. *Journal of Magnetic Resonance Imaging, 14*(2), 156–163.
55. Hoskin, P. J., Carnell, D. M., Taylor, N. J., Smith, R. E., Stirling, J. J., Daley, F. M., Saunders, M. I., Bentzen, S. M., Collins, D. J., d'Arcy, J. A., & Padhani, A. P. (2007). Hypoxia in prostate cancer: Correlation of BOLD-MRI with pimonidazole immunohistochemistry-initial observations. [Research Support, Non-U.S. Gov't]. *International Journal of Radiation Oncology, Biology, Physics, 68*(4), 1065–1071. https://doi.org/10.1016/j.ijrobp.2007.01.018.
56. Hallac, R. R., Ding, Y., Yuan, Q., McColl, R. W., Lea, J., Sims, R. D., Weatherall, P. T., & Mason, R. P. (2012). Oxygenation in cervical cancer and normal uterine cervix assessed using blood oxygenation level-dependent (BOLD) MRI at 3T. *NMR in Biomedicine, 25*(12), 1321–1330. https://doi.org/10.1002/nbm.2804.
57. Jiang, L., Weatherall, P. T., McColl, R. W., Tripathy, D., & Mason, R. P. (2013). Blood oxygenation level-dependent (BOLD) contrast magnetic resonance imaging (MRI) for prediction of breast cancer chemotherapy response: A pilot study. *Journal of Magnetic Resonance Imaging, 37*(5), 1083–1092. https://doi.org/10.1002/jmri.23891.
58. Rijpkema, M., Kaanders, J. H., Joosten, F. B., van der Kogel, A. J., & Heerschap, A. (2002). Effects of breathing a hyperoxic hypercapnic gas mixture on blood oxygenation and vascularity of head-and-neck tumors as measured by magnetic resonance imaging. *International Journal of Radiation Oncology, Biology, Physics, 53*(5), 1185–1191.
59. Jiang, L., McColl, R., Weatherall, P., Tripathy, D., & Mason, R. P. (2005). Blood oxygenation level dependent (BOLD) contrast MRI for early evaluation of breast cancer chemotherapy. *Breast Cancer Research and Treatment, 94*, S257–S258.
60. Zhao, D. W., Pacheco-Torres, J., Hallac, R. R., White, D., Peschke, P., Cerdan, S., et al. (2015). Dynamic oxygen challenge evaluated by NMR T-1 and T-2* - insights into tumor oxygenation. *NMR in Biomedicine, 28*(8), 937–947. https://doi.org/10.1002/nbm.3325.
61. Arias-Ramos, N., Pacheco-Torres, J., & López-Larrubia, P. (2019). Magnetic resonance imaging approaches for predicting the response to hyperoxic radiotherapy in glioma-bearing rats. *OBM. Neurobiology, 3*(1), 18. https://doi.org/10.21926/obm.neurobiol.1901020.
62. Little, R. A., Jamin, Y., Boult, J. K. R., Naish, J. H., Watson, Y., Cheung, S., Holliday, K. F., Lu, H., McHugh, D. J., Irlam, J., West, C. M. L., Betts, G. N., Ashton, G., Reynolds, A. R., Maddineni, S., Clarke, N. W., Parker, G. J. M., Waterton, J. C., Robinson, S. P., & O'Connor, J. P. B. (2018). Mapping hypoxia in renal carcinoma with oxygen-enhanced MRI: Comparison with intrinsic susceptibility MRI and pathology. *Radiology, 288*(3), 739–747. https://doi.org/10.1148/radiol.2018171531.
63. Zhou, H. L., Hallac, R. R., Yuan, Q., Ding, Y., Zhang, Z. W., Xie, X. J., et al. (2017). Incorporating oxygen-enhanced MRI into multi-parametric assessment of human prostate cancer. *Diagnostics, 7*(3), 48. https://doi.org/10.3390/diagnostics7030048.
64. Hectors, S. J., Wagner, M., Bane, O., Besa, C., Lewis, S., Remark, R., et al. (2017). Quantification of hepatocellular carcinoma heterogeneity with multiparametric magnetic resonance imaging. *Science Reporter, 7*, 2452. https://doi.org/10.1038/S41598-017-02706-Z.
65. Kodibagkar, V. D., Cui, W. N., Merritt, M. E., & Mason, R. P. (2006). Novel H-1 NMR approach to quantitative tissue oximetry using hexamethyldisiloxane. *Magnetic Resonance in Medicine, 55*(4), 743–748. https://doi.org/10.1002/mrm.20826.
66. Mason, R. P., Zhao, D., Pacheco-Torres, J., Cui, W., Kodibagkar, V. D., Gulaka, P. K., et al. (2010). Multimodality imaging of hypoxia in preclinical settings. *Quarterly Journal of Nuclear Medicine and Molecular Imaging, 54*(3), 259–280.
67. Agarwal, S., Shankar, R. V., Inge, L. J., & Kodibagkar, V. (2015). MRI assessment of changes in tumor oxygenation post hypoxia-targeted therapy. *Medical Imaging 2015: Biomedical Applications in Molecular, Structural, and Functional Imaging*, 9417. https://doi.org/10.1117/12.2083926.
68. Shibata, T., Giaccia, A. J., & Brown, J. M. (2000). Development of a hypoxia-responsive vector for tumor-specific gene therapy. *Gene Therapy, 7*(6), 493–498. https://doi.org/10.1038/sj.gt.3301124.
69. Vordermark, D., Shibata, T., & Brown, J. M. (2001). Green fluorescent protein is a suitable reporter of tumor hypoxia despite an oxygen requirement for chromophore formation. *Neoplasia, 3*(6), 527–534. https://doi.org/10.1038/sj.neo.7900192.
70. Raman, V., Artemov, D., Pathak, A. P., Winnard, P. T., McNutt, S., Yudina, A., et al. (2006). Characterizing vascular parameters in hypoxic regions: A combined magnetic resonance and optical imaging study of a human prostate cancer model. *Cancer Research, 66*(20), 9929–9936. https://doi.org/10.1158/0008-5472.CAN-06-0886.
71. Krishnamachary, B., Penet, M. F., Nimmagadda, S., Mironchik, Y., Raman, V., Solaiyappan, M., Semenza, G. L., Pomper, M. G., & Bhujwalla, Z. M. (2012). Hypoxia regulates CD44 and its variant isoforms through HIF-1 alpha in triple negative breast cancer. *PLoS One, 7*(8), e44078. https://doi.org/10.1371/journal.pone.0044078.
72. Danhier, P., Krishnamachary, B., Bharti, S., Kakkad, S., Mironchik, Y., & Bhujwalla, Z. M. (2015). Combining optical reporter proteins with different half-lives to detect temporal evolution of hypoxia and reoxygenation in tumors. *Neoplasia, 17*(12), 871–881. https://doi.org/10.1016/j.neo.2015.11.007.
73. Zackrisson, S., van de Ven, S. M., & Gambhir, S. S. (2014). Light in and sound out: Emerging translational strategies for photoacoustic imaging. *Cancer Research, 74*(4), 979–1004. https://doi.org/10.1158/0008-5472.CAN-13-2387.
74. Neuschmelting, V., Burton, N. C., Lockau, H., Urich, A., Harmsen, S., Ntziachristos, V., & Kircher, M. F. (2016). Performance of a multispectral optoacoustic tomography (MSOT) system equipped with 2D vs. 3D handheld probes for potential clinical translation. *Photoacoustics, 4*(1), 1–10. https://doi.org/10.1016/j.pacs.2015.12.001.
75. Goh, Y., Balasundaram, G., Moothanchery, M., Attia, A., Li, X. T., Lim, H. Q., et al. (2018). Multispectral optoacoustic tomography in assessment of breast tumor margins during breast-conserving surgery: A first-in-human case study. *Clinical Breast Cancer, 18*(6), E1247–E1250. https://doi.org/10.1016/j.clbc.2018.07.026.
76. Becker, A., Masthoff, M., Claussen, J., Ford, S. J., Roll, W., Burg, M., Barth, P. J., Heindel, W., Schäfers, M., Eisenblätter, M., & Wildgruber, M. (2018). Multispectral optoacoustic tomography of the human breast: Characterisation of healthy tissue and malignant lesions using a hybrid ultrasound-optoacoustic approach. *European Radiology, 28*(2), 602–609. https://doi.org/10.1007/s00330-017-5002-x.
77. Overgaard, J., Overgaard, M., Nielsen, O. S., Pedersen, A. K., & Timothy, A. R. (1982). A comparative investigation of nimorazole and misonidazole as hypoxic radiosensitizers in a C3h mammary-carcinoma Invivo. *British Journal of Cancer, 46*(6), 904–911. https://doi.org/10.1038/Bjc.1982.300.

78. Tap, W., Papai, Z., van Tine, B., Attia, S., Ganjoo, K., Jones, R. L., et al. (2016). Randomized phase 3, multicenter, open-label study comparing evofosfamide (Evo) in combination with doxorubicin (D) vs. D alone in patients (pts) with advanced soft tissue sarcoma (STS): Study TH-CR-406/SARC021. *Annals of Oncology*, *27*. https://doi.org/10.1093/annonc/mdw388.1.
79. Van Cutsem, E., Lenz, H. J., Furuse, J., Tabernero, J., Heinemann, V., Ioka, T., et al. (2016). Evofosfamide (TH-302) in combination with gemcitabine in previously untreated patients with metastatic or locally advanced unresectable pancreatic ductal adenocarcinoma: Primary analysis of the randomized, double-blind phase III MAESTRO study. *Journal of Clinical Oncology*, *34*(4). https://doi.org/10.1200/jco.2016.34.4_suppl.193.
80. Higgins, J. P., Sarapa, N., Kim, J., & Poma, E. (2018). Unexpected pharmacokinetics of evofosfamide observed in phase III MAESTRO study. *Journal of Clinical Oncology*, *36*(15). https://doi.org/10.1200/Jco.2018.36.15_Suppl.2568.
81. Haider, S., McIntyre, A., van Stiphout, R. G. P. M., Winchester, L. M., Wigfield, S., Harris, A. L., et al. (2016). Genomic alterations underlie a pan-cancer metabolic shift associated with tumour hypoxia. *Genome Biology, 17*, 140. https://doi.org/10.1186/S13059-016-0999-8.
82. Siano, M., Espeli, V., Mach, N., Bossi, P., Licitra, L., Ghielmini, M., Frattini, M., Canevari, S., & de Cecco, L. (2018). Gene signatures and expression of miRNAs associated with efficacy of panitumumab in a head and neck cancer phase II trial. *Oral Oncology, 82*, 144–151. https://doi.org/10.1016/j.oraloncology.2018.05.013.
83. Eustace, A., Mani, N., Span, P. N., Irlam, J. J., Taylor, J., Betts, G. N. J., Denley, H., Miller, C. J., Homer, J. J., Rojas, A. M., Hoskin, P. J., Buffa, F. M., Harris, A. L., Kaanders, J. H. A. M., & West, C. M. L. (2013). A 26-gene hypoxia signature predicts benefit from hypoxia-modifying therapy in laryngeal cancer but not bladder cancer. *Clinical Cancer Research, 19*(17), 4879–4888. https://doi.org/10.1158/1078-0432.CCR-13-0542.
84. Salem, A., Asselin, M. C., Reymen, B., Jackson, A., Lambin, P., West, C. M. L., et al. (2018). Targeting hypoxia to improve non-small cell lung cancer outcome. *Jnci-Journal of the National Cancer Institute, 110*(1), 14–30. https://doi.org/10.1093/jnci/djx160.
85. Workman, P., Aboagye, E. O., Chung, Y. L., Griffiths, J. R., Hart, R., Leach, M. O., Maxwell, R. J., McSheehy, P., Price, P. M., Zweit, J., & Cancer Research UK Pharmacodynamic/Pharmacokinetic Technologies Advisory Committee. (2006). Minimally invasive pharmacokinetic and pharmacodynamic technologies in hypothesis-testing clinical trials of innovative therapies. *Journal of the National Cancer Institute, 98*(9), 580–598. https://doi.org/10.1093/jnci/djj162.
86. Stadlbauer, A., Zimmermann, M., Bennani-Baiti, B., Helbich, T. H., Baltzer, P., Clauser, P., et al. (2018). Development of a non-invasive assessment of hypoxia and neovascularization with magnetic resonance imaging in benign and malignant breast tumors: Initial Results. *Molecular Imaging and Biology*. https://doi.org/10.1007/s11307-018-1298-4.
87. Wegner, C. S., Hauge, A., Simonsen, T. G., Gaustad, J. V., Andersen, L. M. K., & Rofstad, E. K. (2018). DCE-MRI of sunitinib-induced changes in tumor microvasculature and hypoxia: A study of pancreatic ductal adenocarcinoma xenografts. [Research Support, Non-U.S. Gov't]. *Neoplasia, 20*(7), 734–744. https://doi.org/10.1016/j.neo.2018.05.006.
88. Tomaszewski, M. R., Gonzalez, I. Q., O'Connor, J. P., Abeyakoon, O., Parker, G. J., Williams, K. J., Gilbert, F. J., & Bohndiek, S. E. (2017). Oxygen enhanced optoacoustic tomography (OE-OT) reveals vascular dynamics in murine models of prostate cancer. [Research Support, Non-U.S. Gov't]. *Theranostics, 7*(11), 2900–2913. https://doi.org/10.7150/thno.19841.
89. Kakkad, S. M., Penet, M. F., Akhbardeh, A., Pathak, A. P., Solaiyappan, M., Raman, V., et al. (2013). Hypoxic tumor environments exhibit disrupted collagen I fibers and low macromolecular transport. *Plos One, 8*(12), e81869. https://doi.org/10.1371/journal.pone.0081869.
90. Penet, M. F., Kakkad, S., Pathak, A. P., Krishnamachary, B., Mironchik, Y., Raman, V., Solaiyappan, M., & Bhujwalla, Z. M. (2017). Structure and function of a prostate cancer dissemination-permissive extracellular matrix. *Clinical Cancer Research, 23*(9), 2245–2254. https://doi.org/10.1158/1078-0432.CCR-16-1516.
91. Bharti, S. K., Kakkad, S., Danhier, P., Wildes, F., Penet, M. F., Krishnamachary, B., & Bhujwalla, Z. M. (2019). Hypoxia patterns in primary and metastatic prostate cancer environments. *Neoplasia, 21*(2), 239–246. https://doi.org/10.1016/j.neo.2018.12.004.
92. da Ponte, K. F., Berro, D. H., Collet, S., Constans, J. M., Emery, E., Valable, S., & Guillamo, J. S. (2017). *In vivo* relationship between hypoxia and angiogenesis in human glioblastoma: A multimodal imaging study. *Journal of Nuclear Medicine, 58*(10), 1574–1579. https://doi.org/10.2967/jnumed.116.188557.
93. Ayuso, J. M., Gillette, A., Lugo-Cintron, K., Acevedo-Acevedo, S., Gomez, I., Morgan, M., et al. (2018). Organotypic microfluidic breast cancer model reveals starvation-induced spatial-temporal metabolic adaptations. *Ebiomedicine, 37*, 144–157. https://doi.org/10.1016/j.ebiom.2018.10.046.
94. Shah, T., Krishnamachary, B., Wildes, F., Mironchik, Y., Kakkad, S. M., Jacob, D., et al. (2015). HIF isoforms have divergent effects on invasion, metastasis, metabolism and formation of lipid droplets. *Oncotarget, 6*(29), 28104–28119. https://doi.org/10.18632/oncotarget.4612.
95. Bharti, S. K., Mironchik, Y., Wildes, F., Penet, M. F., Goggins, E., Krishnamachary, B., et al. (2018). Metabolic consequences of HIF silencing in a triple negative human breast cancer xenograft. *Oncotarget, 9*(20), 15326–15339. https://doi.org/10.18632/oncotarget.24569.
96. Frantz, C., Stewart, K. M., & Weaver, V. M. (2010). The extracellular matrix at a glance. *Journal of Cell Science, 123*(Pt 24), 4195–4200. https://doi.org/10.1242/jcs.023820.
97. Casazza, A., Di Conza, G., Wenes, M., Finisguerra, V., Deschoemaeker, S., & Mazzone, M. (2014). Tumor stroma: A complexity dictated by the hypoxic tumor microenvironment. *Oncogene, 33*(14), 1743–1754. https://doi.org/10.1038/onc.2013.121.
98. Guadall, A., Orriols, M., Alcudia, J. F., Cachofeiro, V., Martinez-Gonzalez, J., & Rodriguez, C. (2011). Hypoxia-induced ROS signaling is required for LOX up-regulation in endothelial cells. *Frontiers in Bioscience (Elite Edition), 3*, 955–967.
99. Krishnamachary, B., Berg-Dixon, S., Kelly, B., Agani, F., Feldser, D., Ferreira, G., et al. (2003). Regulation of colon carcinoma cell invasion by hypoxia-inducible factor 1. *Cancer Research, 63*(5), 1138–1143.
100. Petrova, V., Annicchiarico-Petruzzelli, M., Melino, G., & Amelio, I. (2018). The hypoxic tumour microenvironment. *Oncogenesis, 7*(1), 10. https://doi.org/10.1038/s41389-017-0011-9.
101. Postovit, L. M., Abbott, D. E., Payne, S. L., Wheaton, W. W., Margaryan, N. V., Sullivan, R., Jansen, M. K., Csiszar, K., Hendrix, M. J. C., & Kirschmann, D. A. (2008). Hypoxia/reoxygenation: A dynamic regulator of lysyl oxidase-facilitated breast cancer migration. *Journal of Cellular Biochemistry, 103*(5), 1369–1378. https://doi.org/10.1002/jcb.21517.
102. Jiang, D., & Lim, S. Y. (2016). Influence of immune myeloid cells on the extracellular matrix during cancer metastasis. *Cancer Microenvironment, 9*(1), 45–61. https://doi.org/10.1007/s12307-016-0181-6.

103. Wang, Y., Wang, H., Li, J., Entenberg, D., Xue, A., Wang, W., & Condeelis, J. (2016). Direct visualization of the phenotype of hypoxic tumor cells at single cell resolution *in vivo* using a new hypoxia probe. *Intravital, 5*(2), e1187803. https://doi.org/10.1080/21659087.2016.1187803.
104. Provenzano, P. P., Eliceiri, K. W., Campbell, J. M., Inman, D. R., White, J. G., & Keely, P. J. (2006). Collagen reorganization at the tumor-stromal interface facilitates local invasion. *Bmc Medicine, 4*, 38. https://doi.org/10.1186/1741-7015-4-38.
105. Yan, Y. M., Zuo, X. S., & Wei, D. Y. (2015). Concise review: Emerging role of CD44 in cancer stem cells: A promising biomarker and therapeutic target. *Stem Cells Translational Medicine, 4*(9), 1033–1043. https://doi.org/10.5966/sctm.2015-0048.
106. Smith, S. J., Diksin, M., Chhaya, S., Sairam, S., Estevez-Cebrero, M. A., & Rahman, R. (2017). The invasive region of glioblastoma defined by 5ALA guided surgery has an altered cancer stem cell marker profile compared to central tumour. *International Journal of Molecular Sciences, 18*(11), 2452. https://doi.org/10.3390/Ijms18112452.
107. Fiaschi, T., Giannoni, E., Taddei, M. L., Cirri, P., Marini, A., Pintus, G., et al. (2013). Carbonic anhydrase IX from cancer-associated fibroblasts drives epithelial-mesenchymal transition in prostate carcinoma cells. *Cell Cycle, 12*(11), 1791–1801. https://doi.org/10.4161/cc.24902.
108. Scholer-Dahirel, A., Costa, A., & Mechta-Grigoriou, F. (2013). Control of cancer-associated fibroblast function by oxidative stress: A new piece in the puzzle. [Comment]. *Cell Cycle, 12*(14), 2169. https://doi.org/10.4161/cc.25547.
109. Nakao, M., Ishii, G., Nagai, K., Kawase, A., Kenmotsu, H., Kon-No, H., et al. (2009). Prognostic significance of carbonic anhydrase IX expression by cancer-associated fibroblasts in lung adenocarcinoma. [Research Support, Non-U.S. Gov't]. *Cancer, 115*(12), 2732–2743. https://doi.org/10.1002/cncr.24303.
110. Nakamura, H., Ichikawa, T., Nakasone, S., Miyoshi, T., Sugano, M., Kojima, M., Fujii, S., Ochiai, A., Kuwata, T., Aokage, K., Suzuki, K., Tsuboi, M., & Ishii, G. (2018). Abundant tumor promoting stromal cells in lung adenocarcinoma with hypoxic regions. *Lung Cancer, 115*, 56–63. https://doi.org/10.1016/j.lungcan.2017.11.013.
111. Lee, S. H., Mcintyre, D., Honess, D., Hulikova, A., Pacheco-Torres, J., Cerdan, S., et al. (2018). Carbonic anhydrase IX is a pH-stat that sets an acidic tumour extracellular pH *in vivo*. *British Journal of Cancer, 119*(5), 622–630. https://doi.org/10.1038/s41416-018-0216-5.
112. Ray, K. J., Simard, M. A., Larkin, J. R., Coates, J., Kinchesh, P., Smart, S. C., Higgins, G. S., Chappell, M., & Sibson, N. (2019). Tumour pH and protein concentration contribute to the signal of amide proton transfer magnetic resonance imaging. *Cancer Research*. https://doi.org/10.1158/0008-5472.CAN-18-2168.
113. Bhujwalla, Z. M., Kakkad, S., Chen, Z., Jin, J., Hapuarachchige, S., Artemov, D., & Penet, M. F. (2018). Theranostics and metabolotheranostics for precision medicine in oncology. *Journal of Magnetic Resonance, 291*, 141–151. https://doi.org/10.1016/j.jmr.2018.03.004.
114. Song, G., Cheng, L., Chao, Y., Yang, K., & Liu, Z. (2017). Emerging nanotechnology and advanced materials for cancer radiation therapy. [Review]. *Adv Mater, 29*(32). https://doi.org/10.1002/adma.201700996.
115. Lau, J., Lin, K. S., & Benard, F. (2017). Past, present, and future: Development of theranostic agents targeting carbonic anhydrase IX. [Review Research Support, Non-U.S. Gov't]. *Theranostics, 7*(17), 4322–4339. https://doi.org/10.7150/thno.21848.
116. Iikuni, S., Ono, M., Watanabe, H., Shimizu, Y., Sano, K., & Saji, H. (2018). Cancer radiotheranostics targeting carbonic anhydrase-IX with (111)In- and (90)Y-labeled ureidosulfonamide scaffold for SPECT imaging and radionuclide-based therapy. *Theranostics, 8*(11), 2992–3006. https://doi.org/10.7150/thno.20982.
117. Chen, Y., Bian, X., Aliru, M., Deorukhkar, A. A., Ekpenyong, O., Liang, S., et al. (2018). Hypoxia-targeted gold nanorods for cancer photothermal therapy. *Oncotarget, 9*(41), 26556–26571. https://doi.org/10.18632/oncotarget.25492.
118. Alsaab, H. O., Sau, S., Alzhrani, R. M., Cheriyan, V. T., Polin, L. A., Vaishampayan, U., Rishi, A. K., & Iyer, A. K. (2018). Tumor hypoxia directed multimodal nanotherapy for overcoming drug resistance in renal cell carcinoma and reprogramming macrophages. *Biomaterials, 183*, 280–294. https://doi.org/10.1016/j.biomaterials.2018.08.053.
119. Meng, X. Q., Zhang, J. L., Sun, Z. H., Zhou, L. H., Deng, G. J., Li, S. P., et al. (2018). Hypoxia-triggered single molecule probe for high-contrast NIR II/PA tumor imaging and robust photothermal therapy. *Theranostics, 8*(21), 6025–6034. https://doi.org/10.7150/thno.26607.
120. Hua, L., Wang, Z., Zhao, L., Mao, H., Wang, G., Zhang, K., Liu, X., Wu, D., Zheng, Y., Lu, J., Yu, R., & Liu, H. (2018). Hypoxia-responsive lipid-poly-(hypoxic radiosensitized polyprodrug) nanoparticles for glioma chemo- and radiotherapy. *Theranostics, 8*(18), 5088–5105. https://doi.org/10.7150/thno.26225.
121. Feng, L., Cheng, L., Dong, Z., Tao, D., Barnhart, T. E., Cai, W., Chen, M., & Liu, Z. (2017). Theranostic liposomes with hypoxia-activated prodrug to effectively destruct hypoxic tumors post-photodynamic therapy. *ACS Nano, 11*(1), 927–937. https://doi.org/10.1021/acsnano.6b07525.
122. Chen, Z. H., Penet, M. F., Krishnamachary, B., Banerjee, S. R., Pomper, M. G., & Bhujwalla, Z. M. (2016). PSMA-specific theranostic nanoplex for combination of TRAIL gene and 5-FC prodrug therapy of prostate cancer. *Biomaterials, 80*, 57–67. https://doi.org/10.1016/j.biomaterials.2015.11.048.
123. Hsiao, H. T., Xing, L. G., Deng, X. L., Sun, X. R., Ling, C. C., & Li, G. C. (2014). Hypoxia-targeted triple suicide gene therapy radiosensitizes human colorectal cancer cells. *Oncology Reports, 32*(2), 723–729. https://doi.org/10.3892/or.2014.3238.
124. Kumar, D., New, J., Vishwakarma, V., Joshi, R., Enders, J., Lin, F. C., et al. (2018). Cancer-associated fibroblasts drive glycolysis in a targetable signaling loop implicated in head and neck squamous cell carcinoma progression. *Cancer Research, 78*(14), 3769–3782. https://doi.org/10.1158/0008-5472.CAN-17-1076.
125. Kashima, H., Noma, K., Ohara, T., Kato, T., Katsura, Y., Komoto, S., Sato, H., Katsube, R., Ninomiya, T., Tazawa, H., Shirakawa, Y., & Fujiwara, T. (2019). Cancer-associated fibroblasts (CAFs) promote the lymph node metastasis of esophageal squamous cell carcinoma. *International Journal of Cancer, 144*(4), 828–840. https://doi.org/10.1002/ijc.31953.
126. Donnarumma, E., Fiore, D., Nappa, M., Roscigno, G., Adamo, A., Iaboni, M., et al. (2017). Cancer-associated fibroblasts release exosomal microRNAs that dictate an aggressive phenotype in breast cancer. *Oncotarget, 8*(12), 19592–19608. https://doi.org/10.18632/oncotarget.14752.
127. Paidi, S. K., Rizwan, A., Zheng, C., Cheng, M. L., Glunde, K., & Barman, I. (2017). Label-free Raman spectroscopy detects stromal adaptations in premetastatic lungs primed by breast cancer. *Cancer Research, 77*(2), 247–256. https://doi.org/10.1158/0008-5472.CAN-16-1862.
128. Napel, S., Mu, W., Jardim-Perassi, B. V., Aerts, H. J. W. L., & Gillies, R. J. (2018). Quantitative imaging of cancer in the postgenomic era: Radio(geno)mics, deep learning, and habitats. *Cancer, 124*(24), 4633–4649. https://doi.org/10.1002/cncr.31630.
129. Stasinopoulos, I., Penet, M. F., Krishnamachary, B., & Bhujwalla, Z. M. (2010). Molecular and functional imaging of invasion and metastasis: Windows into the metastatic cascade. *Cancer Biomarkers, 7*(4), 173–188. https://doi.org/10.3233/CBM-2010-0188.
130. Seong, J., Tajik, A., Sun, J., Guan, J. L., Humphries, M. J., Craig, S. E., Shekaran, A., Garcia, A. J., Lu, S., Lin, M. Z., Wang, N., &

Wang, Y. (2013). Distinct biophysical mechanisms of focal adhesion kinase mechanoactivation by different extracellular matrix proteins. *Proceedings of the National Academy of Sciences of the United States of America, 110*(48), 19372–19377. https://doi.org/10.1073/pnas.1307405110.

131. Polacheck, W. J., Zervantonakis, I. K., & Kamm, R. D. (2013). Tumor cell migration in complex microenvironments. *Cellular and Molecular Life Sciences, 70*(8), 1335–1356. https://doi.org/10.1007/s00018-012-1115-1.

132. Sulzmaier, F. J., Jean, C., & Schlaepfer, D. D. (2014). FAK in cancer: Mechanistic findings and clinical applications. *Nature Reviews. Cancer, 14*(9), 598–610. https://doi.org/10.1038/nrc3792.

133. Yoon, H., Dehart, J. P., Murphy, J. M., & Lim, S. T. (2015). Understanding the roles of FAK in cancer: Inhibitors, genetic models, and new insights. *The Journal of Histochemistry and Cytochemistry, 63*(2), 114–128. https://doi.org/10.1369/0022155414561498.